Study of the structural transition and hydrogenation of CeTiGe

Tadhg Mahon, Sophie Tencé, Rainer Pöttgen, Bernard Chevalier, Etienne Gaudin

Study of the structural transition and hydrogenation of CeTiGe

Tadhg Mahon[a], Sophie Tencé[a], Rainer Pöttgen[b], Bernard Chevalier[a] and Etienne Gaudin[a*]

[a]CNRS, Université Bordeaux, ICMCB, UMR 5026, F-33600 Pessac, France
[b]Institut für Anorganische und Analytische Chemie, Universität Münster, Corrensstrasse 30, D-48149 Münster,Germany

[*]etienne.gaudin@u-bordeaux.fr

Abstract

There remains some disagreement in the literature on CeTiGe over the presence of a structural transition from the low temperature CeFeSi-type form to the high temperature CeScSi-type structure. We present a detailed study of the effect of temperature on this structural transition. Furthermore, the same hydride is obtained after hydrogenation of both forms. Using neutron powder diffraction we find that the structure of $CeTiGeH_{1.5}$ corresponds to a stuffed variant of the CeScSi-type structure with space group *I*4/*mmm*, a = 4.0785(1) Å and c = 17.1060(8) Å. The H atoms occupy both the Ce_4 tetrahedral sites and the $CeTi_4$ square based pyramidal sites for a total hydrogen occupancy of 1.5 H f.u.$^{-1}$. Preliminary examinations of the magnetic properties after hydrogenation reveal the onset of low temperature magnetic order around 3.5 K, suggesting for the first time a hydrogen induced magnetic order for an intermetallic with CeScSi-type structure.

Keywords

intermetallics; structural transition; hydrogen insertion; magnetism

1. Introduction

A wide range of ternary *RTX* compounds (*R* = rare earth, *T* = transition metal or Mg and *X* = *p*-block element) crystallizing in the CeFeSi structure type are known. Examples include *R*CoSi [1], *R*CoGe [2], RMnSi [3-4], *R*FeSi [5], *R*RuSi [6] and many more [7]. Layers of empty [R_4] tetrahedra are observed in this structure-type (figure 1) and the filling of these interstitial sites by hydrogen atoms induces a very interesting modulation of the physical properties [8]. These *RTX*H hydrides adopt the ZrCuSiAs-type structure which is also observed for LaFePO [9], the first member of the new family of iron-based superconductors. The changes in the physical properties are dependent on the competition between the expansion of the unit-cell volume induced by the H absorption and the *R*-H bonding. Among the changes observed one can cite the transitions from antiferromagnetic to intermediate valence behavior for CeCoSi and CeCoSiH, respectively [10-11], from heavy fermion (CeRuSi) to antiferromagnetic behavior for CeRuSiH [12,13] and the huge influence of hydrogenation on the antiferromagnetic properties of the Nd- and Mn- substructures of NdMnSi [4]. Very recently, the new hydride LaFeSiH, obtained through hydrogen insertion in the Pauli paramagnetic phase LaFeSi [5], displays superconductivity with onset at 11 K [14].

There are also many examples of compounds that crystallize in the related CeScSi structure type, an ordered variant of the La_2Sb-type (figure 1), such as *R*ScSi or *R*ScGe [15–18], *R*MgSn [19–21], *R*MgPb [22,23] and *R*ZrSb [24]. The CeFeSi and CeScSi-type structures are closely related (see [25] for instance) and both exhibit a layer of empty [R_4] tetrahedra. Hydrogenation of CeScSi [26], GdTiGe [25] and NdSc*X* (*X* = Si, Ge) [16] shows a drastic decrease or a disappearance of the magnetic ordering. To date only the *R*TiGe compounds where *R* = Ce [27,28], Sm [28-29], Gd [25, 29-30] and Tb [31-32] have been shown to adopt both structure types. Morozkin *et al* [29] have shown that the starting composition plays a role in stabilizing one form over another or a mixture of the two. They found that sub-stoichiometric amounts of Ti stabilized the CeScSi form, that the CeFeSi form could be stabilized by sub-stoichiometric amounts of Ge and that a sub-stoichiometric Gd composition stabilized a mixture of the two structure types. Moreover, an increase of the size of the rare-earth in the *R*TiGe germanides leads to the stabilization of the CeScSi-type structure. The same trend is observed in the *R*ScSb series [33] where the CeScSi-type structure is stabilized with the lighter rare-earths (*R* = La-Nd, Sm) and the CeFeSi-type with heavier rare-earth (*R* = Gd-Tm, Lu, Y).

There remains a conflict in the literature around the structural transition in CeTiGe. Chevalier *et al.* [27] describe a high temperature structural transition from the CeFeSi to CeScSi structure types for this compound by annealing at 1373 K. However, while studying the

magnetic properties of this material, Deppe *et al.* [34] found that even the samples that were annealed at 1423 K retained the CeFeSi type structure. To date no further studies have been carried out on this material to define the exact conditions of the structural transition in CeTiGe. In this work we thus present the results of a detailed study of the temperature dependence of the transition from the CeFeSi to the CeScSi structure type for CeTiGe. Furthermore we will present the effects of hydrogen insertion into the CeFeSi and CeScSi-type forms of CeTiGe on its structural and magnetic properties. The crystal structure of the hydride was determined from neutron diffraction measurements.

2. Experiments

Following the results of Chevalier *et al.* [27], CeTiGe samples were prepared with an atomic ratio of 32.5:34.5:33 (Ce and Ti, Strem Chemicals 99.9%, Ge Alfa Aesar 99.999%). A slight excess of Ti was used to avoid the presence of the ferromagnetic phase Ce_5Ge_3 [35]. The elements were melted together under argon in an electric arc furnace with a water cooled hearth. A Ti getter was used to absorb any residual oxygen before melting the sample and weight losses were generally below 1 %. Parts of the resulting samples were then annealed in evacuated quartz ampoules at 1173 K for two weeks as both block sample and pellets of compacted powder (referred to as powder samples) after grinding of the as-cast sample. Sample purity was checked by powder X-ray diffraction before and after annealing.

In order to investigate the temperature dependence of the structural transition, block and compacted powder samples were wrapped in Ta foil and sealed in evacuated quartz ampoules. Subsequent annealing was performed at 1173, 1273 and 1373 K for 3 days. Samples were quenched in both water and air.

Hydrogenation of CeTiGe was performed *via* solid-gas reaction in a hermetically sealed hydrogenation container (H_2-gas AlphaGaz N5.0, 99.999%). The sample was heated to 623 K and kept at this temperature for 2 hours under active vacuum to activate the surface. After activation, the sample was hydrogenated under 5 bar of H_2 gas at the same temperature for 12 h.

Routine powder X-ray diffraction (XRD) was performed with the use of a Philips 1050-diffractometer (Cu-K_α radiation) for the structural characterization and phase identification of the as-cast and annealed samples. X-ray powder data for Rietveld analysis were collected at room temperature using a PANalytical X'pert Pro diffractometer working with Cu-$K\alpha_1$ radiation (1.54051 Å) in the range $10 \leq 2\theta \leq 130°$ and a step size of 0.008°. Neutron diffraction measurements of $CeTiGeH_x$ were performed on the 3T2 and on G4.1 beamlines at the Laboratoire Leon Brillouin (LLB), Saclay, France with λ = 1.226 Å and λ = 2.423 Å

respectively. Rietveld refinement and full pattern matchings were carried out using the Fullprof program package [36].

Magnetization measurements were performed using a superconducting quantum interference device (S.Q.U.I.D.) magnetometer (Quantum Design MPMS-XL) in the temperature range 1.8–300 K and applied fields up to 2 T. Heat capacity measurements were performed on a room temperature pressed pellet using a standard relaxation method with a QD PPMS device. A sample of 10.7 mg was glued to the sample holder using Apiezon N-grease. The heat capacity of the sample holder and grease was measured just before the sample was studied. The resistivity was measured on a different pellet between 1.8 and 270 K with a standard four-probe dc method in a PPMS. Because of the low compactness and the presence of microcracks in the pellet, the absolute value of ρ could not be determined accurately; for this reason, a normalized representation ρ(T)/ρ(270 K) is given.

3. Results

3.1. Temperature mediated structural transition in CeTiGe

The initial sample described in this section was annealed at 1173 K for two weeks. Additional heat treatments at higher temperature were performed for three days on different pieces of the initial sample. Figure 2 shows the powder XRD measurements on CeTiGe after the annealing of the powder samples at 1173, 1273 and 1373 K. From the diffraction pattern in Figure 2 it can be seen that, after annealing of a pellet of ground CeTiGe at 1173 K the sample is almost completely single phase CeTiGe in the CeFeSi structure type with only small amounts of Ce_5Ge_3 as a secondary phase. Subsequent annealing of the sample at 1273 K for three days leads to the appearance of a peak at 2θ = 35.75 ° (marked with the symbol **o** in Figure 2). This corresponds to the (105) peak of the CeScSi-type form of CeTiGe as reported in [27] and is only present in this form of the material. Therefore, it can be used as an indicator of the presence of this structural type. At the same time that this peak appears, the peak at 2θ = 31.50 ° (the (102) peak of the CeFeSi-type form, marked with the symbol ×) decreases significantly in intensity after annealing at 1273 K for three days. Rietveld analysis of the diffraction pattern shows 70(1) wt.% of the CeScSi-type and 19(1) wt.% of the CeFeSi-type CeTiGe (and 11 wt.% of Ti_5Ge_3 and Ce_2O_3). Moreover, after annealing for 3 days at 1373 K this (102) peak has completely vanished, indicating the disappearance of the CeFeSi-type form. It is clear, therefore, that the CeFeSi form of CeTiGe is the low temperature form (LT) while the CeScSi form is the high temperature (HT) one. The complete transformation of the sample annealed at 1373 K to the high temperature form is attributed to the accelerated kinetics at higher temperature. This clearly shows that the

structural transition begins somewhere between 1173 and 1273 K. In order to more accurately place the transition temperature, differential scanning calorimetry (DSC) measurements were performed. Unfortunately, due to the slow kinetics of the structural transition, we were unable to observe it using this method. Thus, a more accurate transition temperature than the temperature range 1173-1273 K could not be determined. During these studies of the heat treatment, an investigation was made on the effect of cooling speed by quenching in water and air. It was found that simply removing quickly the samples from the furnace without quenching in water produced very little variation in the HT/LT ratio when compared with quenching in water. Given that quenching from 1273/1373 K in water often causes the quartz tube to crack, exposing the hot sample to water, the samples were all simply quickly removed from the furnace and cooled in air.

Finally, the effect of sample morphology on the structural transition was also investigated. Figure 3 shows the XRD patterns of a block and pellet of the same CeTiGe sample after annealing together in the same furnace at 1373 K for 3 days. The peaks labelled (**o**) are not present in the CeFeSi structure type and the peaks labelled with (×) are not present in the CeScSi structure type. Thus they clearly indicate the presence (or absence) of their respective structural forms. It can clearly be seen that the morphology of the sample (block or pellet) has a significant effect on the structural transition. When the sample is annealed in block form, only a small quantity of the HT CeScSi-type CeTiGe is found whereas the same sample, when annealed in identical conditions as a pellet of compacted powder, results in an almost total conversion to the high temperature form. This is likely due to strain created during the structural transition which causes a shifting of two consecutive unit cells of CeFeSi by $a/2 + b/2$. This strain is accompanied by a slight increase of the volume per formula unit V/Z from 67.4 [28] to 68.5 $Å^3$ [27] (+ 1.6%) when going from the LT to the HT form. It can be assumed that in the block sample, the surrounding crystal resists the crystallographic changes associated with this structural transition. On the contrary, in the powder form, the smaller crystallites and high porosity would allow the structure to change more easily, facilitating the transition. These results explain why Deppe *et al*. did not observe the CeScSi form of CeTiGe during a first study in which they annealed ingots, without grinding, at 1273 K and without fast cooling of the samples [37]. In a second study [34], even if neither the exact composition they used for their synthesis nor the form of their samples is provided, they do state that they introduced substitutions of Zr and Nb for Ti and small amounts of Si on the Ge sites. The study of the effect of composition in [29] showed that at least 30 % substitution of Zr or Nb is required on the Ti site to stabilize the CeScSi-form and that low levels of Si substitution on the Ge site (10 %) preserves the coexistence of both forms.

According to the available data on the experiment performed in ref [34] it is conceivable that they should see a coexistence of the two phases. However, if they performed their annealing on blocks rather than powdered samples, it would explain the lack of any observed high temperature form. They suggest in this paper that the CeScSi-type structure is connected with off stoichiometry. However, the structural refinement of the CeScSi-type structures of GdTiGe[29], CeTiGe[27] phases and of the corresponding hydrides GdTiGeH[25] and $CeTiGeH_x$ (see below) didn't show any off-stoichiometry.

3.2 Hydrogenation of CeTiGe

The XRD patterns of the HT and LT-forms of CeTiGe and their hydrides are shown in Figure 4 (left) and (right) respectively. After hydrogenation of the HT form we observe a decrease in the *a* unit cell parameter from 4.15447(9) to 4.0889(2) Å and a large increase in the *c* parameter from 15.8814(4) to 16.9917(9) Å without a change in the symmetry. Interestingly, the same structural form is obtained for the hydride whether starting from the HT or the LT form. However, the hydride formed from the low temperature analogue shows a change in the unit cell parameters of a = 4.14440(1) to 4.0899(1) Å and c = 7.9309(1) ($2c$ = 15.8618 Å) to 17.0018(2) Å with much broader XRD peaks than the HT analogue. A strong decrease of the crystallite size after hydrogenation is observed in both cases with a more deleterious effect on the crystallinity when beginning from the LT form. After hydrogenation, the crystallite size (calculated using the Voigt approximation implemented in Fullprof [36], the instrumental resolution function being determined with a LaB_6 standard) is decreasing from 283(1) to 45(1) nm for the LT-form and from 636(5) to 76(1) nm for the HT-form. Thus, the structural transition that normally requires extended treatment of several days at very high temperatures (1373 K) can be realized at much lower temperatures (623 K) and much more quickly (several hours) during the course of the hydrogenation reaction. This structural change on hydrogenation is similar to that observed for the hydrogenation of the CeFeSi-form of GdTiGe [25].

3.3 Neutron diffraction on $CeTiGeH_x$

Neutron diffraction was carried out on $CeTiGeH_x$ to determine the amount of hydrogen inserted as well as its location within the unit cell. The initial refinement was performed based on the known structure of the CeScSi-type hydrides, with hydrogen in the 4*d* Wyckoff position (0, 1/2, 1/4), *i.e.* inside the rare earth tetrahedral sites. The resulting fit was of medium quality indicating that the hydrogen atoms likely occupy another site(s). A number of empirical rules have been established which can help us in predicting the location of hydrogen atoms in a crystal structure [38]. In order to accept hydrogen, an interstitial site must have a radius of at least 0.4 Å

[39,40] and not exceeding 0.8 Å [41]. By considering the crystal structure of the HT form of CeTiGe from [27] we see that the available sites for hydrogen insertion are the Ce_4 tetrahedra, the Ti_4Ce_2 octahedra and the Ti_4Ge_2 octahedra with a maximum radius of the corresponding interstitial site equal to 0.56, 0.61 and 0.45 Å, respectively (the atomic radii used for calculation are taken from [39,40] and references therein). These rules also state that sites containing the *p* block elements are less favorable for H insertion than sites containing elements that form stronger bonds with hydrogen such as the rare earth elements [41]. Indeed hydrogen is found to occupy interstitial sites that are most distant from the *p* block elements [42]. Based on these rules we can predict that the Ti_4Ce_2 octahedral sites will be preferentially filled over the Ti_4Ge_2 ones. Fourier difference analysis (Figure 5) illustrates clearly a residual, negative, nuclear density around the (0, 0, 1/2) position, inside the Ti_4Ce_2 octahedra as predicted. This suggests the presence of H atoms which have a negative coherent neutron scattering length of b_C (H) = –3.74 fm [43].

In light of this, a second hydrogen position was added to the refinement at the (0, 0, 1/2) position with full occupancy which resulted in a significant improvement of the fit. However, this produced unreasonably large B_{iso} values for the H2 site. For the final refinement, we shifted the hydrogen atoms slightly out of the (0, 0, 1/2) plane to the 4*e* Wyckoff site and found a refined position of (0, 0, 0.521(1)) with an occupancy of 0.47(1). The occupancy factor for the H1 position has been refined in the same time and converged to the value 1.02(2) and then has been fixed to 1. The slight shift of the H2 position from the center of the Ti_4Ce_2 octahedron is coherent with the elongation along the ***c***-direction of the residues observed in the Fourier difference map for the H2 position (Figure 5). The final refinement converged well and is shown in Figure 6 with reliability factors R_{Bragg} = 7.9%, R_p/R_{wp} = 20.3%/16.7% and a respective amount of 94.9(1) % and 5.1(1) % for $CeTiGeH_{1.47(1)}$ and the secondary phase Ti_5Ge_3. The small amount of Ti_5Ge_3 observed in the sample is consistent with the starting stoichiometry which shows a slight excess of Ti and Ge to avoid the presence of the magnetic secondary phase Ce_5Ge_3. The crystal structure parameters are gathered in **Table 1**. The half occupancy of the 4*e* site stems from the close proximity of neighbouring sites that would result in too short H–H distances if both were filled. Thus CeTiGe can absorb 1.5 atoms of hydrogen per formula unit with the hydrogen atoms occupying the vacant rare earth tetrahedral sites as well as the $CeTi_4$ square-pyramidal sites formed from the Ti_4 square plane and one Ce atom. Similar square-pyramidal sites have been seen in another CeScSi-type hydrides [16 and references therein]. The crystal structure of the filled hydride $CeTiGeH_{1.47(1)}$ is depicted in Figure 1. The structural transition from the CeFeSi-type to the CeScSi-type on hydrogen insertion is believed to be due to an

increased stability of the CeScSi-type hydride. This is also observed in the hydrogenation of the GdTiGe system by [25]. However, GdTiGe absorbs only one atom of H f.u.$^{-1}$, suggesting that only the Gd_4 tetrahedra are occupied. Thus the structural transition cannot simply be due to the availability of the second site for hydrogen. Moreover, the filling of this second site by hydrogen cannot be predicted from structural considerations. Indeed, in the case of HT-CeTiGe and HT-GdTiGe, the distances between the center C_{Oh} of the Ti_4R_2 octahedra (R = Ce or Gd) and the atoms at the tops are long enough in both cases to allow the insertion of hydrogen. The Ti–C_{Oh} and Gd–C_{Oh} distances are equal to 2.033 and 2.705 Å in GdTiGe and the Ti–C_{Oh} and Ce–C_{Oh} distances are equal to 2.075 and 2.765 Å in CeTiGe. These distances are longer than the corresponding distances in the binary hydrides TiH_2 [44], CeH_2 [45] and GdH_2 [46] with $d_{Ti–H}$ = 1.929 Å, $d_{Ce–H}$ = 2.417 Å and $d_{Gd–H}$ = 2.296 Å.

The hydrogenation of HT-CeTiGe causes a number of changes in the interatomic distances given in **Table 2**. The two Ce–Ce distances are affected differently. The shortest Ce–Ce distance increases from 3.806 to 3.837 Å while the longer one (also equal to the *a* parameter) decreases from 4.149 to 4.0785 Å. The shorter one of these is larger than the Ce–Ce distance in metallic Ce ($d_{Ce–Ce}$= 3.636 Å [47]) but comparable to the distances in other Ce intermetallics such as CeMnSi ($d_{Ce–Ce}$ = 3.772 Å [3]). The H insertion induces a regularization of the Ce_4 tetrahedra as seen from the ratio of the two side lengths which increases from 0.92 to 0.94 on hydrogenation (ideal ratio = 1.00). At the same time, the [TiGe] layers contract and the distance between the Ce and [TiGe] planes (equal to *c*/4) increases, namely from 3.98 to 4.28 Å. Thus hydrogenation causes an overall increase in the 2D character of the substructure of CeTiGe. In the [TiGe] layer of CeTiGe the Ti–Ti distances of 2.934 Å are very close to those seen in *hcp* Ti metal of 2.94 Å [47]. Hydrogenation causes a slight contraction of these distances to 2.884 Å and also of the Ti–Ge distances from 2.767 to 2.694 Å, close to the Ti–Ge distance present in other compounds such as $TiGe_2$ ($d_{Ti–Ge}$ = 2.591 Å [48]) and NiTiGe ($d_{Ti–Ge}$ = 2.627 Å [49]). The distance from the centre of the tetrahedra to the Ce atoms ($d_{Ce–Td/H1}$) decreases slightly on hydrogenation from 2.403 to 2.400 Å. $d_{Ce–H1}$ = 2.400 Å is similar to the distance seen in CeH_2 of 2.417 Å [45], indicating strong Ce–H bonding. The $d_{Ce–H2}$ = 2.698 Å in $CeTiGeH_{1.5}$ is larger than that in CeH_2, suggesting that the Ce–H2 interactions are weaker than the Ce–H1 ones. Meanwhile, the distance between the Ti atoms and the H2 position, equal to 2.063 Å is comparable to the Ti–H distance in TiH_2 of 1.929 Å [44]. The location of the second H atom in the square-pyramidal site rather than the octahedron was also seen in our recent study of $NdScSiH_{1.5}$ [16] where the displacement of the H (D) atom is likely driven by a more favorable bonding distance between H and Nd. A similar argumentation may be applied here. By considering the H2 atom in the centre of the

octahedral site, we calculate $d_{Ce–H2}$ of 3.011 Å and $d_{Ti–H2}$ = 2.039 Å. The former of these is too long for good Ce–H interactions. Thus by moving out of the square plane and into the square-pyramidal site, Ce–H bonding can be facilitated while not significantly changing the Ti–H distances.

3.4 Magnetic properties of CeTiGe and $CeTiGeH_{1.5}$

As Ce compounds have been shown to exhibit interesting changes in their magnetic properties on hydrogenation [8, 10-13, 50], we have investigated the magnetic properties of the $CeTiGeH_{1.5}$ samples. Both forms of the pristine material are known to be non-ordered heavy fermion systems with a Curie-Weiss paramagnetic behavior and an effective magnetic moment consistent with the Ce^{3+} ion [27, 34, 37, 51]. This confirms that the Ti is non-magnetic in these systems. With a Kondo temperature $T_K \approx 50$ K and a Sommerfeld coefficient $\gamma \approx 0.3$ $Jmol^{-1}K^{-2}$, the LT form of CeTiGe is considered to be located to the non-magnetic side of the quantum critical point within the Doniach diagram. Additionally it presents a first-order metamagnetic transition at moderate field connected with some kind of localization of the 4f(Ce) electrons [34]. Going from the LT to the HT form results in the decrease of the hybridization between 4f(Ce) and conduction electrons but no magnetic order is observed down to 2 K despite an upturn of the specific heat curve at low temperature[27].

The magnetization measurement against temperature on $CeTiGeH_{1.5}$ is shown in Figure 7 in the temperature range 1.8-15 K. The M/H curve in zero-field cooling (ZFC) is presented for two different samples, sample 2 being the one that has been used for neutron diffraction. As shown in inset of Figure 7, the hydride is a Curie-Weiss paramagnet with a Curie-Weiss temperature θ = –1.4 K (θ = -16 K for sample 2) and an effective moment of 2.39 μ_B $f.u.^{-1}$ (2.37 μ_B $f.u.^{-1}$ for sample 2) which is close to the value for the free Ce^{3+} ion (2.54 μ_B). The difference is mainly ascribed to the presence of secondary phases as well as the downward curvature at lower temperature due to the crystal field effect (the effective moment is found equal to 2.50 μ_B $f.u.^{-1}$ for a fit done above T = 180 K). Although negative, the Curie-Weiss temperature is too small to conclude about the dominant magnetic interactions. At lower temperature, the magnetization curve displays a maximum around T_N = 3.5 K for sample 1 and sample 2, suggesting the occurrence of an antiferromagnetic transition. In fact, the anomaly is more or less visible on the M(T) curves of the different samples we synthesized, depending on the nature and the amount of the secondary phases. In particular, the presence of the dense Kondo compound Ce_5Ge_3, detected in some samples and showing a ferromagnetic behavior below 10 K [35], can hamper the observation of a distinct maximum. However, the transition is clearly confirmed by the specific

heat measurement presented in Figure 8, which shows a well-defined peak at 3.6 K. Likewise, the transition is observed on the electrical resistivity (inset of Figure 8) by a sudden drop of ρ(T) below 4 K. This reduction of the resistivity is characteristic as electron scattering from magnetic fluctuations is suppressed. At higher temperature, the ρ(T) curve follows a weak linear decrease down to 50 K, then a broad drop sets in below 30 K. This decrease of ρ(T) is the signature of the formation of a coherent Kondo lattice as observed in the pristine CeTiGe samples [27, 37]. Therefore, the hydrogenation of CeTiGe yields an apparent decrease of the Kondo interaction since the hydride $CeTiGeH_{1.5}$ seems to have switched to the left side of the Doniach diagram. However, the exact nature of the magnetic order could not be determined since the neutron diffraction data do not evidence a substantial magnetic contribution down to 1.5 K. The reason of this result remains unclear but, as the lowest angle of measurement was 2θ=7°, it is possible that the significant magnetic peaks are not visible, especially if the Ce magnetic moment is weak. It is noticeable that magnetic peaks in the neutron pattern for the isostructural hydride $NdScSiH_{1.5}$ were also absent at low temperature, despite the observation of a magnetic transition around 4 K [16].

5. Conclusion

CeTiGe possesses two modifications: a CeFeSi-type phase, corresponding to the low temperature structure, and a CeScSi-type phase at high temperatures. The transition between the two modifications occurs slowly, starting in the temperature range 1173-1273 K. The transition is significantly faster in powder samples than in block samples, likely due to the small particle size and high porosity in the powder samples which permits the structural changes more easily. CeTiGe can absorb 1.5 atoms of H $f.u.^{-1}$, neutron diffraction confirming the localisation of H atoms in the Ce_4 tetrahedra and the Ti_4Ce square-pyramidal sites. Hydrogenation causes the onset of low temperature magnetic order, most likely antiferromagnetic, but the exact type of magnetic order will require further work to be confirmed. In contrast to what was observed after hydrogenation of homologous phases [16, 25-26, 52] with a drastic decrease of the magnetic ordering temperature, the insertion of hydrogen into CeTiGe led to the appearance of a magnetic ordering. In this case, hydrogenation plays the role of a negative pressure, tuning the system from the non-magnetic to the magnetic domain of the Doniach phase diagram.

Acknowledgments

The authors thank the Laboratoire Léon Brillouin (LLB) for the provision of beamtime at 3T2 and G41, G. André and F. Porcher for help with the neutron experiments. They also thank R. Decourt for specific heat and resistivity measurements performed in ICMCB.

Table 1. Atomic Coordinates and Isotropic Atomic Displacement Parameters (Å^2) of $CeTiGeH_{1.47(1)}$ Determined from Neutron Diffraction data. Space Group *I*4/*mmm*, *a* = 4.0785(1) and *c* = 17.1060(8) Å.

Atom	Wyckoff	*x*	*y*	*z*	Occ.	U_{iso} (Å^2)
Ce	4*e*	0	0	0.3240(3)	1	0.0116(3)
Ti	4*c*	0	1/2	0	1	0.021(5)
Ge	4*e*	0	0	0.1029(2)	1	0.0073(8)
H1	4*d*	0	1/2	1/4	1	0.032(4)
H2	4*e*	0	0	0.518(1)	0.47(1)	0.022(3)

Table 2. Number of neighbours and interatomic distances in HT-CeTiGe (X-ray)[27] and $CeTiGeH_{1.47(1)}$ (neutron diffraction) in Å.

Atom 1		Atom 2/site	d (Å)	
			CeTiGe (HT)	$CeTiGeH_{1.47(1)}$
Ce	**4**	**H1/*Td*†**	*2.403*	2.400(3)
	1	**H2/*SP*‡**	*2.447*	2.698(15)
	4	**Ge**	3.079	3.143(3)
	1	**Ge**	3.358	3.782(6)
	4	**Ti**	3.457	3.636(5)
	4	**Ce**	3.806	3.837(7)
	4	**Ce**	4.149	4.0785(1)
Ti	**4**	**H2/*SP*‡**	*2.099*	2.063(3)
	4	**Ge**	2.767	2.694(3)
	4	**Ti**	2.934	2.88391(9)
Ge	**4**	**H1/*Td*†**	*2.985*	3.239(3)
	1	**H2/*SP*‡**	*3.301*	3.2226(7)
H1/*Td*°	**4**	**H1/*Td*†**	*2.934*	2.88391(9)
H2/*SP*#	**1**	**H2/*SP*‡**	*0.64*	0.63(3)

†Hypothetical position (0, 1/2, 1/4) in Tetrahedral Site (*Td*) for HT-CeTiGe

‡Hypothetical position (0, 0, 0.52) in Square-pyramidal site (*SP*) for HT-CeTiGe

Figure captions

Figure 1. Crystal structures of LT-CeTiGe (CeFeSi-type, *P*4/*nmm*)[28], HT-CeTiGe (CeScSi-type, *I*4/*mmm*)[27] and $CeTiGeH_{1.5}$ (*I*4/*mmm*, determined from neutron diffraction measurements, see table 1).

Figure 2. Powder X-ray diffraction patterns of CeTiGe after temperature treatment at 1173, 1273 and 1373 K performed on a pellet of compacted powder.

Figure 3. Powder XRD patterns of the same CeTiGe sample after annealing at 1373 K in both pellet (top) and block (bottom) form.

Figure 4. **(**Left) Powder XRD patterns of CeTiGe (HT form), (right) Powder XRD patterns of CeTiGe (LT form) before and after hydrogenation.

Figure 5. Fourier difference map after the refinement of $CeTiGeH_x$ with the H atom located only in the Ce_4 tetrahedral site. ($y = 0$)

Figure 6. Rietveld refinement of the neutron diffraction pattern of $CeTiGeH_{1.47(1)}$ at room temperature (observed (red circles), calculated (black line), and difference (blue line) profiles). The reliability factors R-Bragg, Rp and Rwp are equal to 7.9%, 20.3% and 16.7%, respectively.

Figure 7. Temperature dependence of the magnetization divided by the magnetic field of $CeTiGeH_{1.5}$ (sample 1 and sample 2). The inset shows the inverse susceptibility versus T fitted with a Curie-Weiss type law.

Figure 8. Temperature dependence of the specific heat of $CeTiGeH_{1.5}$. Inset: Temperature dependence of the electrical resistivity ρ/ρ_{270K} normalized at 270 K.

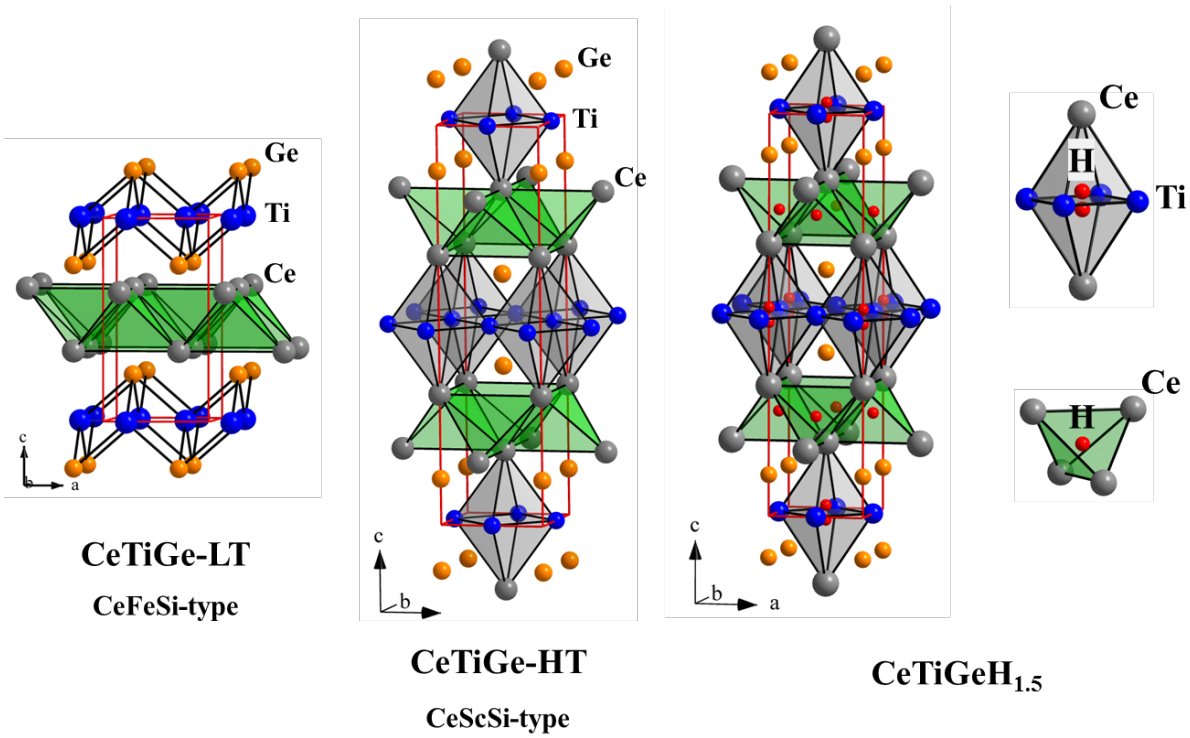

Figure 1. Crystal structures of LT-CeTiGe (CeFeSi-type, *P*4/*nmm*)[28], HT-CeTiGe (CeScSi-type, *I*4/*mmm*) [27] and $CeTiGeH_{1.5}$ (*I*4/*mmm*, determined from neutron diffraction measurements, see table 1).

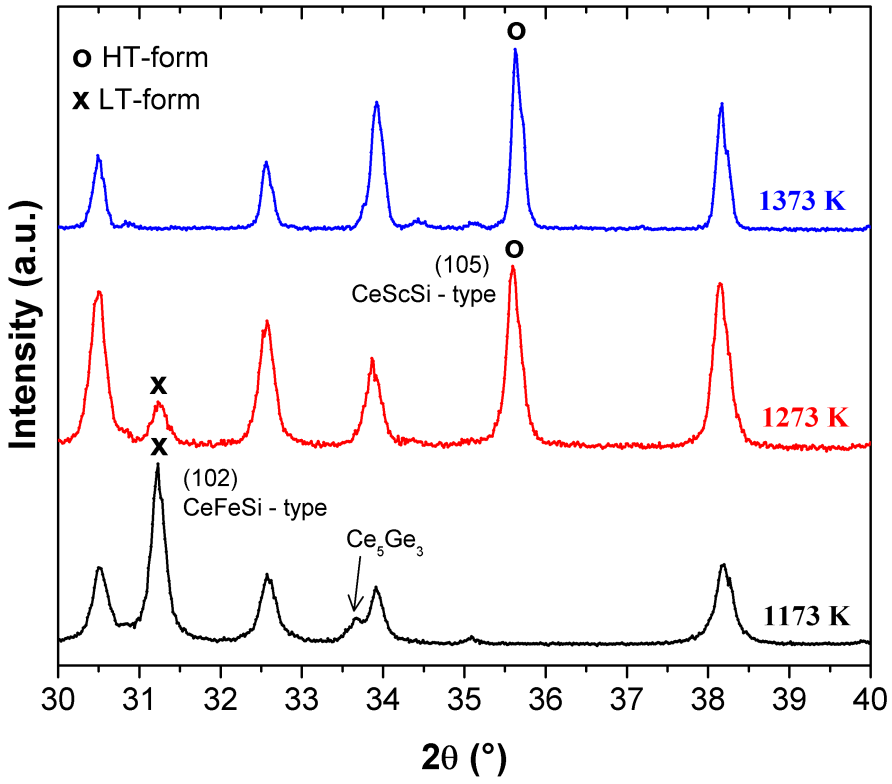

Figure 2. Powder X-ray diffraction patterns of CeTiGe after temperature treatment at 1173, 1273 and 1373 K performed on a pellet of compacted powder.

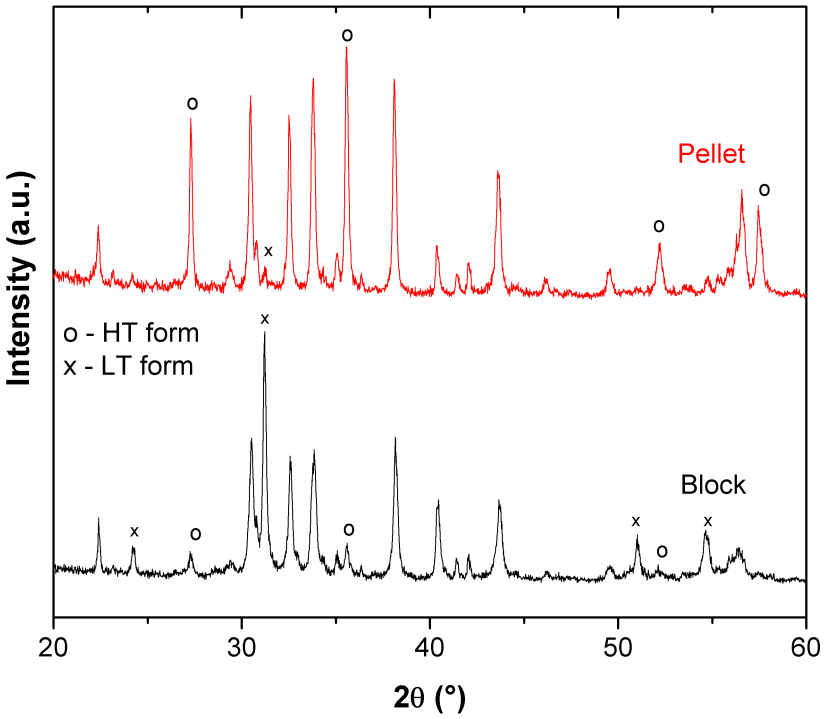

Figure 3. Powder XRD patterns of the same CeTiGe sample after annealing at 1373 K in both pellet (top) and block (bottom) form.

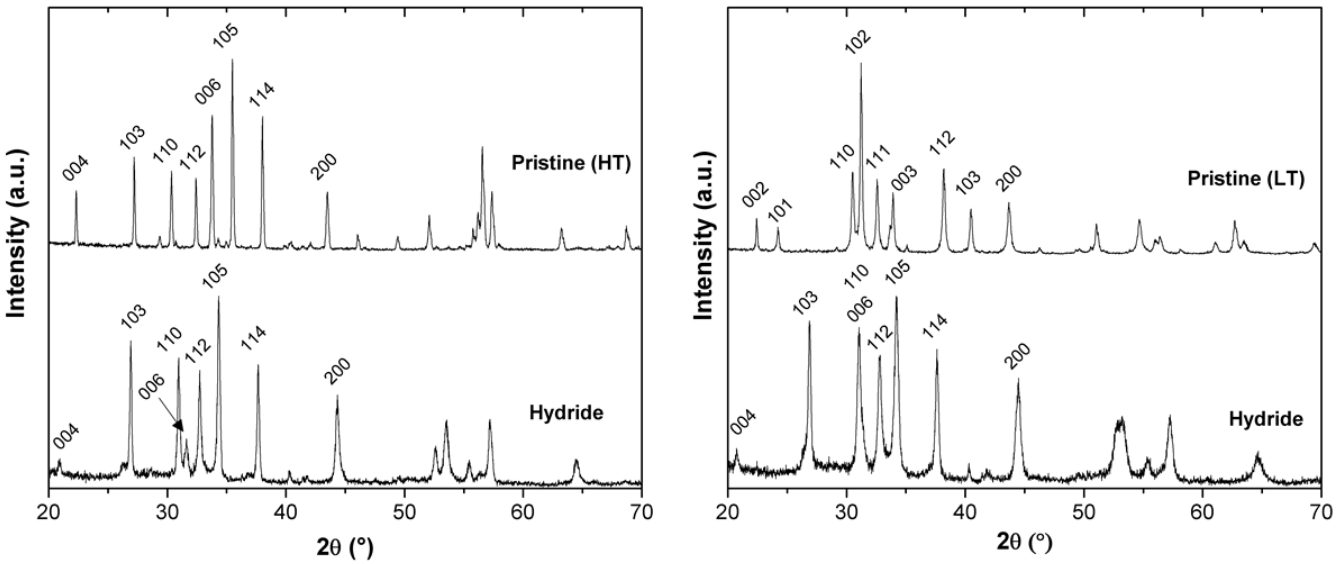

Figure 4. (Left) Powder XRD patterns of CeTiGe (HT form), (right) Powder XRD patterns of CeTiGe (LT form) before and after hydrogenation.

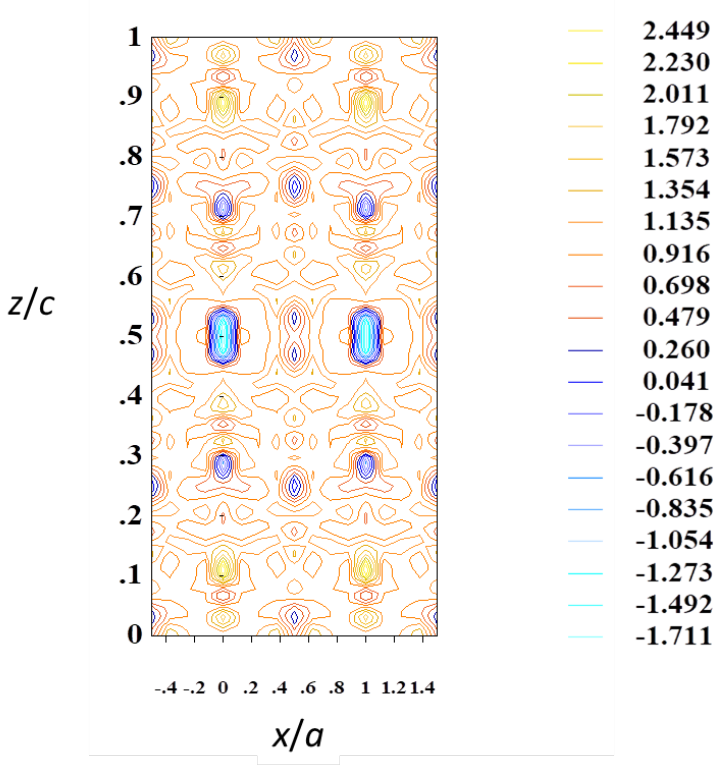

Figure 5. Fourier difference map after the refinement of $CeTiGeH_x$ with the H atom located only in the Ce_4 tetrahedral site. ($y = 0$)

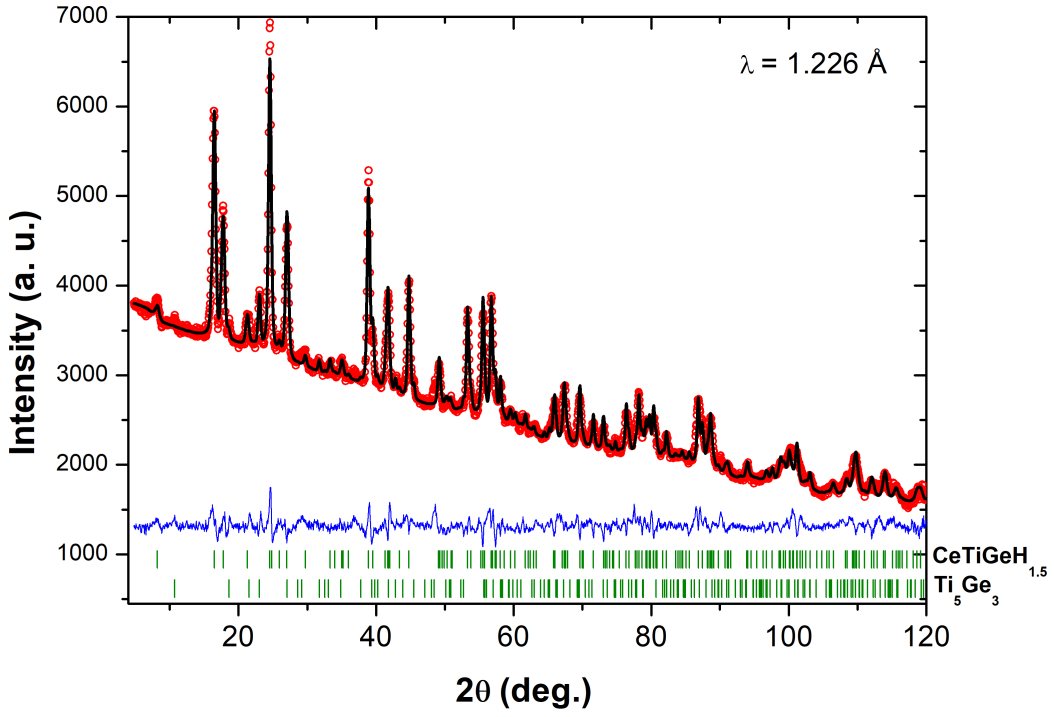

Figure 6. Rietveld refinement of the neutron diffraction pattern of $CeTiGeH_{1.47(1)}$ at room temperature (observed (red circles), calculated (black line), and difference (blue line) profiles). The reliability factors R-Bragg, Rp and Rwp are equal to 7.9%, 20.3% and 16.7%, respectively.

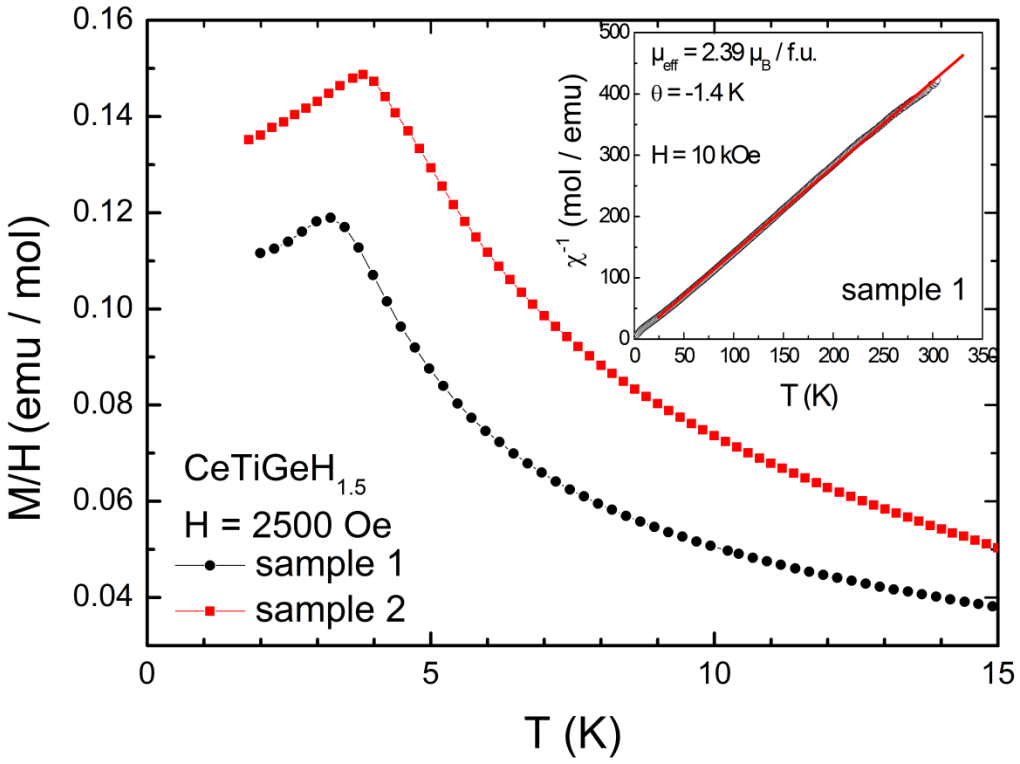

Figure 7. Temperature dependence of the magnetization divided by the magnetic field of $CeTiGeH_{1.5}$ (sample 1 and sample 2) measured in zero-field cooling (ZFC). The inset shows the inverse susceptibility versus T fitted with a Curie-Weiss type law.

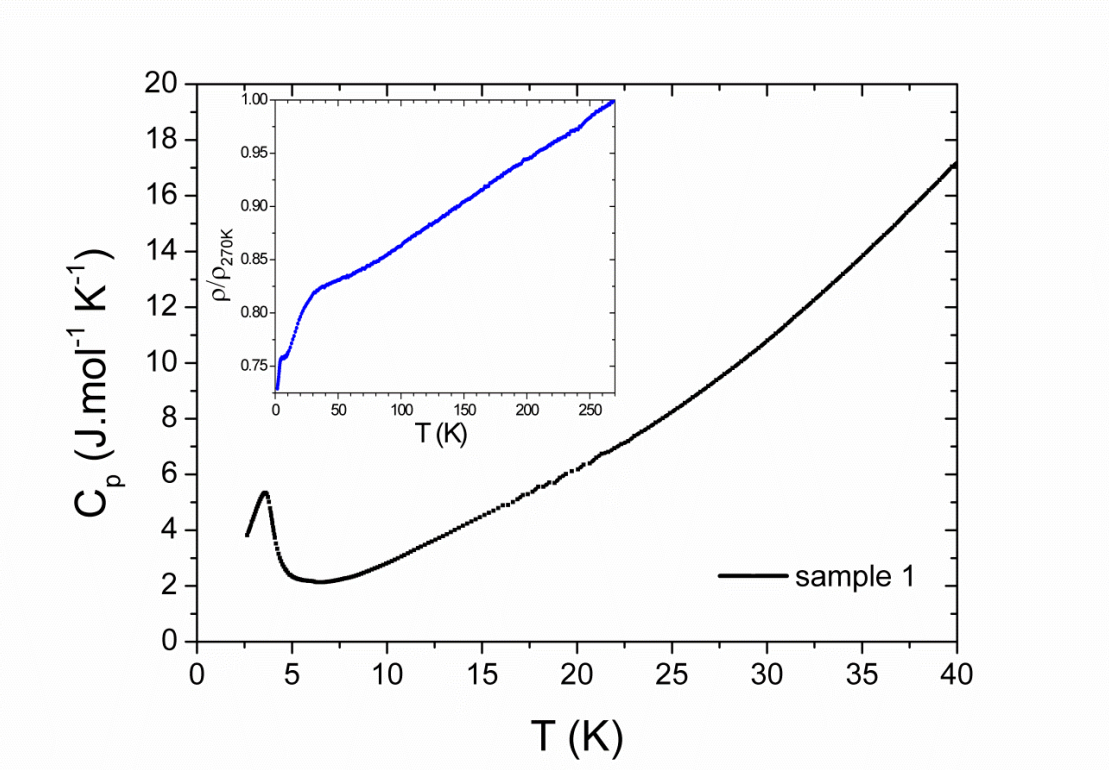

Figure 8. Temperature dependence of the specific heat of $CeTiGeH_{1.5}$. Inset: Temperature dependence of the electrical resistivity ρ/ρ_{270K} normalized at 270 K.

References

[1] R. Welter, G. Venturini, E. Ressouche, B. Malaman, Magnetic properties of RCoSi (R = La-Sm, Gd, Tb) compounds from susceptibility measurements and neutron diffraction studies, J. Alloys Compd. 210 (1994) 279–286. doi:16/0925-8388(94)90150-3. doi.org/10.1016/0925-8388(94)90150-3.

[2] R. Welter, G. Venturini, B. Malaman, E. Ressouche, Crystallographic data and magnetic properties of new RCoGe (R =-La-Nd) compounds from susceptibility measurements and neutron diffraction study, J. Alloys Compd. 201 (1993) 191–196. doi.org/10.1016/0925-8388(93)90883-O.

[3] R. Welter, G. Venturini, B. Malaman, High rare earth sublattice ordering temperatures in RMnSi compounds (R = La-Sm, Gd) studied by susceptibility measurements and neutron diffraction, J. Alloys Compd. 206 (1994) 55–71. doi:10.1016/0925-8388(94)90011-6.

[4] S. Tencé, G. André, E. Gaudin, P. Bonville, A. F. Al Alam, S. F. Matar, W. Hermes, R. Pöttgen, B. Chevalier, Huge influence of hydrogenation on the magnetic properties and structures of the ternary silicide NdMnSi, J. Appl. Phys. 106 (2009) 33910. doi:10.1063/1.3190488.

[5] R. Welter, G. Venturini, B. Malaman, Magnetic properties of RFeSi (R = La-Sm, Gd-Dy) from susceptibility measurements and neutron diffraction studies, J. Alloys Compd. 189 (1992) 49–58. doi:10.1016/0925-8388(92)90045-B.

[6] R. Welter, G. Venturini, B. Malaman, E. Ressouche, Crystallographic data and magnetic properties of new RTX compounds (R = La-Sm, Gd; T = Ru, Os; X = Si, Ge). Magnetic structure of NdRuSi, J. Alloys Compd. 202 (1993) 165–172. doi.org/10.1016/0925-8388(93)90536-V.

[7] S. Gupta, K. G. Suresh, Review on magnetic and related properties of RTX compounds, J. Alloys Compd. 618 (2015) 562–606. doi:10.1016/j.jallcom.2014.08.079.

[8] B. Chevalier, S. Tencé, E. Gaudin, S. F. Matar, J.-L. Bobet, Various magnetic behaviors of the hydrides deriving from the tetragonal CeFeSi-type compounds, J. Alloys Compd. 480 (2009) 43–45. doi:10.1016/j.jallcom.2008.09.183.

[9] Y. Kamihara, H. Hiramatsu, M. Hirano, R. Kawamura, H. Yanagi, T. Kamiya, H. Hosono, Iron-Based Layered Superconductor:~ LaOFeP, J. Am. Chem. Soc. 128 (2006) 10012–10013. doi:10.1021/ja063355c.

[10] B. Chevalier, S. F. Matar, J. Sanchez Marcos, J. Rodriguez Fernandez, From antiferromagnetic ordering to spin fluctuation behavior induced by hydrogenation of ternary compounds CeCoSi and CeCoGe, Physica B 378–380 (2006) 795–796. doi:10.1016/j.physb.2006.01.291.

[11] B. Chevalier, S. F. Matar, Effect of H insertion on the magnetic, electronic, and structural properties of CeCoSi, Phys. Rev. B 70 (2004) 174408. doi:10.1103/physrevb.70.174408.

[12] B. Chevalier, E. Gaudin, S. Tencé, B. Malaman, J. R. Fernandez, G. André, B. Coqblin, Hydrogenation inducing antiferromagnetism in the heavy-fermion ternary silicide CeRuSi, Phys. Rev. B 77 (2008) 1–10. doi:10.1103/PhysRevB.77.014414.

[13] S. Tencé, G. André, E. Gaudin, B. Chevalier, Modulated magnetic structures of the antiferromagnetic hydride CeRuSiH, J. Phys.: Condens. Matter. 20 (2008) 255239. doi:10.1088/0953-8984/20/25/255239.

[14] F. Bernardini, G. Garbarino, M. Sulpice, Núñez-Regueiro, E. Gaudin, B. Chevalier, M.-A. Méasson, A. Cano, S. Tencé, Iron-based superconductivity extended to the novel silicide LaFeSiH, Phys. Rev. B 97 (2018) 100504(R). doi.org/10.1103/PhysRevB.97.100504.

[15] A. Oleaga, V. Liubachko, P. Manfrinetti, A. Provino, Y. Vysochanskii, A. Salazar, Critical behavior study of NdScSi, NdScGe intermetallic compounds, J. Alloys Compd. 723 (2017) 559–

566. doi:10.1016/j.jallcom.2017.06.289.

[16] S. Tencé, T. Mahon, E. Gaudin, B. Chevalier, J.-L. Bobet, R. Flacau, B. Heying, U. C. Rodewald, R. Pöttgen, Hydrogenation studies on NdScSi and NdScGe, J. Solid State Chem. 242 (2016) 168–174. doi:10.1016/j.jssc.2016.02.017.

[17] S. K. Singh, S. K. Dhar, P. Manfrinetti, A. Palenzona, D. Mazzone, High magnetic transition temperatures in RScT (R = Pr, Nd and Sm; T = Si and Ge) compounds: Multiple spin reorientations in PrScGe, J. Magn. Magn. Mater. 269 (2004) 113–121. doi:10.1016/S0304-8853(03)00583-3.

[18] S. Tencé, O. Isnard, E. Gaudin, B. Chevalier, Synthesis and magnetic properties of the ternary germanide TbScGe, J. Alloys Compd. 560 (2013) 195–199. doi.org/10.1016/j.jallcom.2013.02.002.

[19] P. Manfrinetti, A. Provino, K. A. Gschneidner, Jr., On the RMgSn rare earth compounds, J. Alloys Compd. 482 (2009) 81–85. doi:10.1016/j.jallcom.2009.03.178.

[20] P. Lemoine, A. Vernière, J. F. Marêché, B. Malaman, Magnetic properties of the ternary RMgSn (R = Pr, Nd, Sm, Gd–Tm): First series of antiferromagnetic CeScSi-type structure compounds, J. Alloys Compd. 508 (2010) 9–13. doi:10.1016/j.jallcom.2010.08.020.

[21] C. Ritter, A. Provino, P. Manfrinetti, K. A. Gschneidner, Jr., The magnetic structures of RMgSn compounds (R = Ce, Pr, Nd, Tb), J. Alloys Compd. 509 (2011) 9724–9732. doi:10.1016/j.jallcom.2011.07.100.

[22] A. Provino, K. A. Gschneidner, Jr., P. Manfrinetti, Structure and thermal stability of the RMgPb rare earth compounds, and the anomalous melting behaviour of SmMgPb, J. Alloys Compd. 497 (2010) 131–138. doi:10.1016/j.jallcom.2010.03.083.

[23] P. Lemoine, A. Vernière, G. Venturini, J. F. Marêché, S. Capelli, B. Malaman, Magnetic properties and magnetic structures of the CeScSi-type RMgPb (R = Ce-Nd, Sm, Gd-Tm) compounds, J. Magn. Magn. Mater. 324 (2012) 2937–2952. doi:10.1016/j.jmmm.2012.03.037.

[24] A. V. Morozkin, I. A. Sviridov, New ternary CeScSi-type RZrSb compounds (R = Y, Gd-Tm, Lu), J. Alloys Compd. 320 (2001) 2–3. doi:10.1016/S0925-8388(01)00943-4.

[25] E. Gaudin, S. F. Matar, R. Pöttgen, M. Eul, B. Chevalier, Drastic Change of the Ferromagnetic Properties of the Ternary Germanide GdTiGe through Hydrogen Insertion, Inorg. Chem. 50 (2011) 11046–11054. doi:10.1021/ic201579r.

[26] B. Chevalier, W. Hermes, B. Heying, U. C. Rodewald, A. Hammerschmidt, S. F. Matar, E. Gaudin, R. Pöttgen, New Hydrides REScSiH and REScGeH (RE = La, Ce): Structure, magnetism, and chemical bonding, Chem. Mater. 22 (2010) 5013–5021. doi:10.1021/cm101290f.

[27] B. Chevalier, W. Hermes, E. Gaudin, R. Pöttgen, New high temperature modification of CeTiGe: structural characterization and physical properties, J. Phys.: Condens. Matter. 22 (2010) 146003. doi:10.1088/0953-8984/22/14/146003.

[28] A. V. Morozkin, Y. D. Seropegin, I. A. Sviridov, New ternary CeFeSi-type RTiGe (R = La, Ce, Sm) compounds, J. Alloys Compd. 285 (1999) L5-L7. doi:10.1016/S0925-8388(98)01046-9.

[29] A. V. Morozkin, L. M. Viting, I. A. Sviridov, I. A. Tskhadadze, CeScSi- and CeFeSi-type structures in compounds derived from GdTiGe, J. Alloys Compd. 297 (2000) 168–175. doi:10.1016/S0925-8388(99)00583-6.

[30] I. A. Tskhadadze, V. V. Chernyshev, A. N. Streletskii, V. K. Portnoy, A. V. Leonov, I.A. Sviridov, I. V. Telegina, V. N. Verbetskii, Y. D. Seropegin, A. V. Morozkin, GdTiGe (CeScSi-type structure) and GdTiGe (CeFeSi-type structure) as the coherent phases with different magnetic

and hydrogenization properties, Mater. Res. Bull. 34 (1999) 1773–1787. doi.org/10.1016/S0025-5408(99)00159-2.

[31] S. A. Nikitin, I. A. Tskhadadze, I. V. Telegina, A. V. Morozkin, Y. D. Seropegin, Magnetic properties of RTiGe compounds, J. Magn. Magn. Mater. 182 (1998) 375–380. doi:10.1016/S0304-8853(97)01036-6.

[32] S. Tence, E. Gaudin, O. Isnard, B. Chevalier, Magnetic and magnetocaloric properties of the high-temperature modification of TbTiGe, J. Phys.: Condens. Matter. 24 (2012) 296002. doi:10.1088/0953-8984/24/29/296002.

[33] A. Provino, D. Paudyal, A. V. Morozkin, P. Manfrinetti, K. A. Gschneidner Jr, Systematics and anomalies in formation and crystal structures of RScSb and $R_3Sc_2Sb_3$ rare earth compounds, J. Alloys Compd. 587 (2014) 783–789. doi.org/10.1016/j.jallcom.2013.10.197.

[34] M. Deppe, S. Lausberg, F. Weickert, M. Brando, Y. Skourski, N. Caroca-Canales, C. Geibel, F. Steglich, Pronounced first-order metamagnetic transition in the paramagnetic heavy-fermion system CeTiGe, Phys. Rev. B 85 (2012). doi:10.1103/physrevB.85.060401.

[35] M. Kurisu, T. Mitsumata, I. Oguro, Dense Kondo compound Ce_5Ge_3, Physica B 259–261 (1999) 96–98. doi:10.1016/S0921-4526(98)01041-2.

[36] J. Rodriguez-Carvajal, Recent Advances in Magnetic Structure Determination by neutron powder diffraction, Physica B 192 (1993) 55–69. doi.org/10.1016/0921-4526(93)90108-I.

[37] M. Deppe, N. Caroca-Canales, S. Hartmann, N. Oeschler, C. Geibel, New non-magnetically ordered heavy-fermion system CeTiGe, J. Phys.: Condens. Matter. 21 (2009) 206001. doi:10.1088/0953-8984/21/20/206001.

[38] H. W. Brinks, V. A. Yartys, B. C. Hauback, Crystal structure of $TbNiSiD_{1.78}$, J. Alloys Compd. 322 (2001) 160–165. doi:10.1016/S0925-8388(01)01013-1.

[39] D. G. Westlake, Site occupancies and stoichiometries in hydrides of intermetallic compounds: Geometric considerations, J. Less Common Met. 90 (1983) 251–273. doi:10.1016/0022-5088(83)90075-9.

[40] D. G. Westlake, Hydrides of intermetallic compounds: A review of stabilities, stoichiometries and preferred hydrogen sites, J. Less Common Met. 91 (1983) 1–20. doi:10.1016/0022-5088(83)90091-7.

[41] V. A. Yartys, I. R. Harris, V. V Panasyuk, Novel metal-hydride materials and technologies: Recent advances and further prospects, Mater. Sci. 33 (1997) 436–449. doi:10.1007/BF02537542.

[42] S. Rundqvist, R. Tellgren, Y. Andersson, Hydrogen and Deuterium in transition metal-p element compounds: crystal chemical aspects of interstitial solubility and hydride phase formation, J. Less Common Met. 101 (1984) 145–168. doi:10.1016/0022-5088(84)90092-4.

[43] V. F. Sears, Neutron scattering lengths and cross sections, Neutron News. 3 (1992) 26–37. doi:10.1080/10448639208218770.

[44] H. L. Yakel, Thermocrystallography of higher hydrides of titanium and zirconium, Acta Crystallogr. 11 (1958) 46–51. doi:10.1107/S0365110X58000098.

[45] C. E. Holley, R. N. R. Mulford, F. H. Ellinger, W. C. Koehier, W. H. Zachariasen, The Crystal Structure of Some Rare Earth Hydrides, J. Phys. Chem. 59 (1955) 1226–1228. doi:10.1021/j150534a010.

[46] M. Ellner, H. Reule, E. J. Mittemeijer, Unit cell parameters and densities of the gadolinium dihydride GdH_{2+x}, J. Alloys Compd. 279 (1998) 179-183. doi:10.1016/S0925-8388(98)00681-1.

[47] N. N. Greenwood, A. Earnshaw, Chemistry of the elements, Butterworth-Heinemann Ltd. (1995) 1423–1449. **ISBN:** 9780750633659.

[48] H. J. Wallbaum, Über intermetallische Germaniumverbindungen, Naturwissenschaften 32 (1944) 76–76. doi:10.1007/BF01468012.

[49] W. Bażela, A. Szytuła, Crystal and magnetic structure of the $NiMn_{1-t}Ti_tGe$ system, Phys. Status Solidi 66 (1981) 45–52. doi:10.1002/pssa.2210660104.

[50] B. Chevalier, S. F. Matar, M. Ménétrier, J. S. Marcos, J. R. Fernandez, J. Rodriguez Fernandez, Influence of Ce-H bonding on the physical properties of the hydrides $CeCoSiH_{1.0}$ and $CeCoGeH_{1.0}$, J. Phys.: Condens. Matter 18 (2006) 6045–56. doi:10.1088/0953-8984/18/26/022.

[51] R. Welter, A. Vernière, G. Venturini, B. Malaman, High rare earth sublattice ordering temperatures in new CeFeSi-type RTiGe (R = La–Nd, Sm) compounds, J. Alloys Compd. 283 (1999) 54–58. doi:10.1016/S0925-8388(98)00904-9.

[52] T. Mahon, E. Gaudin, A. Villesuzanne, R. Decourt, J.-L. Bobet, O. Isnard, B. Chevalier, S. Tencé, Hydrogen Insertion in the Intermetallic GdScGe: A Drastic Reduction of the Dimensionality of the Magnetic and Transport Properties, Inorg. Chem. 57 (2018) 14230−14239.